Towards a Unified Analysis of Brain Maturation and Aging across the Entire Lifespan: A MRI Analysis

Pierrick Coupé,[1,2]* Gwenaelle Catheline,[3] Enrique Lanuza,[4] and José Vicente Manjón[5]; for the Alzheimer's Disease Neuroimaging Initiative

[1]*University of Bordeaux, LaBRI, UMR 5800, PICTURA, Talence, F-33400, France*
[2]*CNRS, LaBRI, UMR 5800, PICTURA, Talence, F-33400, France*
[3]*University of Bordeaux, CNRS, EPHE PSL Research University of, INCIA, UMR 5283, Bordeaux, F-33000, France*
[4]*Department of Cell Biology, University of Valencia, Burjassot, Valencia 46100, Spain*
[5]*Instituto Universitario de Tecnologías de la Información y Comunicaciones (ITACA), Universitat Politècnica de València, Camino de Vera s/n, Valencia 46022, Spain*

Abstract: There is no consensus in literature about lifespan brain maturation and senescence, mainly because previous lifespan studies have been performed on restricted age periods and/or with a limited number of scans, making results instable and their comparison very difficult. Moreover, the use of

Additional Supporting Information may be found in the online version of this article.

Data used in preparation of this article were obtained from the Alzheimer's Disease Neuroimaging Initiative (ADNI) database (adni.loni.usc.edu). As such, the investigators within the ADNI contributed to the design and implementation of ADNI and/or provided data but did not participate in analysis or writing of this report. A complete listing of ADNI investigators can be found at: http://adni.loni.usc.edu/wp-content/uploads/how_to_apply/ADNI_Acknowledgement_List.pdf

Contract grant sponsor: French State (French National Research Ageny in the frame of the Investments for the future Program IdEx Bordeaux); Contract grant number: ANR-10-IDEX-03- 02, HL-MRI Project; Contract grant sponsor: Cluster of excellence CPU and TRAIL (HR-DTI ANR-10-LABX-57); Contract grant sponsor: CNRS ("Defi imag'In and the dedicated volBrain support); Contract grant sponsor: Ministerio de Economia y competitividad (Spanish); Contract grant number: TIN2013-43457-R; Contract grant sponsor: National Institute of Child Health and Human Development; Contract grant number: HHSN275200900018C; Contract grant sponsors: National Institute of Child Health and Human Development, the National Institute on Drug Abuse, the National Institute of Mental Health, and the National Institute of Neurological Disorders and Stroke; Contract grant numbers: N01- HD02-3343, N01-MH9-0002, and N01-NS-9-2314, -2315, -2316, -2317, -2319 and -2320; Contract grant sponsor: National Institutes of Health; Contract grant number: U01 AG024904; Contract grant sponsor: National Institute on Aging and the National Institute of Biomedical Imaging and Bioengineering (ADNI); Contract grant sponsor: NIH; Contract grant number: P30AG010129, K01 AG030514; Contract grant sponsor: Dana Foundation; Contract grant sponsor: OASIS project (OASIS data); Contract grant numbers: P50 AG05681, P01 AG03991, R01 AG021910, P50 MH071616, U24 RR021382, R01 MH56584; Contract grant sponsor: Common-wealth Scientific Industrial Research Organization (a publicly funded government research organization); Contract grant sponsor: Science Industry Endowment Fund, National Health and Medical Research Council of Australia; Contract grant number: 1011689; Contract grant sponsors: Alzheimer's Association, Alzheimer's Drug Discovery Foundation, and an anonymous foundation; Contract grant sponsor: Human Brain Project; Contract grant number: PO1MHO52176-11 (ICBM, P.I. Dr John Mazziotta); Contract grant sponsor: Canadian Institutes of Health Research; Contract grant number: MOP-34996; Contract grant sponsor: U.K. Engineering and Physical Sciences Research Council (EPSRC); Contract grant number: GR/S21533/02; Contract grant sponsor: ABIDE funding resources; Contract grant sponsor: NIMH; Contract grant number: K23MH087770; Contract grant sponsor: Leon Levy Foundation; Contract grant sponsor: NIMH award to MPM; Contract grant number: R03MH096321

*Correspondence to: Pierrick Coupé. E-mail: Pierrick.coupe@u-bordeaux.fr

Received for publication 23 March 2017; Revised 12 July 2017; Accepted 16 July 2017.

DOI: 10.1002/hbm.23743

Published online 24 July 2017 in Wiley Online Library (wileyonlinelibrary.com).

nonharmonized tools and different volumetric measurements lead to a great discrepancy in reported results. Thanks to the new paradigm of BigData sharing in neuroimaging and the last advances in image processing enabling to process baby as well as elderly scans with the same tool, new insights on brain maturation and aging can be obtained. This study presents brain volume trajectory over the entire lifespan using the largest age range to date (from few months of life to elderly) and one of the largest number of subjects ($N = 2{,}944$). First, we found that white matter trajectory based on absolute and normalized volumes follows an inverted U-shape with a maturation peak around middle life. Second, we found that from 1 to 8–10 y there is an absolute gray matter (GM) increase related to body growth followed by a GM decrease. However, when normalized volumes were considered, GM continuously decreases all along the life. Finally, we found that this observation holds for almost all the considered subcortical structures except for amygdala which is rather stable and hippocampus which exhibits an inverted U-shape with a longer maturation period. By revealing the entire brain trajectory picture, a consensus can be drawn since most of the previously discussed discrepancies can be explained. *Hum Brain Mapp 38:5501–5518, 2017*.

Key words: aging; maturation; lifespan; MRI segmentation; patch-based processing; brain trajectory

INTRODUCTION

Brain development and aging are key topics in neuroscience. The study of normal brain maturation and age-related brain atrophy is crucial to better understand normal brain development and a large variety of neurological disorders. With the rise of the population age, it is becoming increasingly important to understand the cognitive changes that accompany aging, both normal and pathologic. Moreover, analyzing brain maturation and senescence during the entire lifespan may help to better understand the undergoing process on normal brain development and aging.

Despite the large number of studies dedicated to brain trajectory analysis over the last decades, an important disagreement remains between existing results [Walhovd et al., 2011, 2016]. Some studies described early life increase of gray matter (GM) volumes followed by a decrease [Giedd et al., 1999; Lenroot et al., 2007; Raznahan et al., 2011] while other works described GM decrease all along the lifespan [Aubert-Broche et al., 2013; Brain Development Cooperative Group, 2012; Ducharme et al., 2016; Mills et al., 2016; Ostby et al., 2009]. An extensive review of these inconstancies can be found in Walhovd et al. [2016]. For white matter (WM) the picture is inverted, with a consensus for the early life period characterized by an increase. However, less consistent effect of age in adulthood has been reported [Fjell et al., 2014; Jernigan et al., 2011]. In addition, time of brain maturation is also different according to the studies [Groeschel et al., 2010; Hedman et al., 2012]. Discrepancies also exist for the shape of trajectories for cortical and subcortical structures, sometimes described as linear, U-shaped (curvilinear) or as more complex polynomial curves. Finally, sometimes sexual dimorphism is described in these studies and sometimes no gender difference is observed [Giedd et al., 1999; Lenroot and Giedd, 2010; Lenroot et al., 2007; Suzuki et al., 2005]. The lack of consensus on brain development and aging prevents us to better understand these highly complex and multifactor phenomena. The significant divergence between existing results is due to many factors.

First, the use of restricted life periods (e.g., childhood [Brain Development Cooperative Group, 2012], adolescence [Lenroot and Giedd, 2010; Vijayakumar et al., 2016], adulthood [Ziegler et al., 2012], etc.) makes difficult the comparison of results, and tends to favor simple models capturing only brain growth or aging. Thus, it prevents global understanding of brain modification across the entire lifespan. Up to now, no study covered the entire lifespan including babies from few months of life to elderly older than 90.

Second, the use of a limited number of scans for certain age range (especially at childhood) may produce unstable results limiting the reproducibility and accuracy of estimations. The large majority of previous studies used less than 100 subjects [Walhovd et al., 2011], some studies used several hundreds of subjects [Brain Development Cooperative Group, 2012; Giedd and Rapoport, 2010; Mills et al., 2016; Ziegler et al., 2012] and very few studies used more than 1,000 subjects [Fjell et al., 2013; Potvin et al., 2016].

In addition, the use of nonharmonized acquisition protocols, segmentation tools, labelling protocols [Walhovd et al., 2016] and volumetric measurements such as absolute volume [Brain Development Cooperative Group, 2012], normalized volumes using intracranial volume [Good et al., 2002; Mills et al., 2016], GM volume [Ziegler et al., 2012], or *z*-scores [Ostby et al., 2009; Walhovd et al., 2011], lead to a great discrepancy in reported results [Walhovd et al., 2011]. Moreover, some studies are based on cross-sectional data while others on longitudinal ones. Consequently, this heterogeneity makes difficult the definition of normative values [Potvin et al., 2016] stressing the need of using harmonized protocols over large samples covering the entire lifespan.

TABLE I. Dataset description

DATASET	Acquisition	Before QC	After QC	Gender after QC	Age in years after QC
C-MIND	1 site with 3T MR scanner	266	236	$F = 129$ $M = 107$	8.44 (4.35) [0.74–18.86]
NDAR	10 sites with 1.5T and 3T MR scanner	612	382	$F = 174$ $M = 208$	12.39 (5.94) [1.08–49.92]
ABIDE	20 sites with 3T MR scanner	528	492	$F = 84$ $M = 408$	17.53 (7.83) [6.50–52.20]
ICBM	1 sites with 1.5T MR scanner	308	294	$F = 142$ $M = 152$	33.75 (14.32) [18–80]
IXI	3 sites with 1.5T and 3T MR scanner	588	573	$F = 321$ $M = 252$	49.52 (16.70) [20.0- 86.2]
OASIS	1 sites with 1.5T MR scanner	315	298	$F = 187$ $M = 111$	45.34 (23.82) [18 - 94]
AIBL	2 sites with 1.5T and 3T MR scanners	236	233	$F = 121$ $M = 112$	72.24 (6.73) [60 - 89]
ADNI 1	51 sites with 1.5T MR scanner	228	223	$F = 108$ $M = 115$	75.96 (5.03) [60 – 90]
ADNI 2	14 sites with 3T MR scanners	215	213	$F = 113$ $M = 100$	74.16 (6.39) [56.3 - 89]
Total	**103 sites with 1.5T and 3T scanners**	**3,296**	**2,944**	**F =1,379 (47%)** **M = 1,565 (53%)**	**39.65 (26.62)** **[0.74 - 94]**

This table provides the name of the dataset, the MR acquisition configuration, the number of considered image before and after QC, the gender proportion after QC and the average mean, standard deviation in parentheses and the interval in brackets.

Finally, the use of an exigent quality control in the whole measurement process plays a major role in the quality of the final estimated brain models. This step is often not considered enough, while the model estimation greatly depends on a careful quality control [Ducharme et al., 2016].

Therefore, one of the most important challenges in neuroscience is to provide a consensual and unified vision of brain maturation and aging. In this study, we have addressed the previously mentioned limiting factors. First, thanks to the new paradigm of BigData sharing in neuroimaging [Poldrack and Gorgolewski, 2014], we have been able to use a very high number of samples ($N = 3{,}296$) covering the largest lifespan period never studied (from few months to advanced age). Moreover, all the considered MRI scans obtained from several freely available databases were processed using the same advanced MRI processing pipeline [Manjon and Coupe, 2016]. Thanks to the last advances in image processing, images from different age ranges can be analyzed with the same tool. To get insight on brain maturation and aging at global (i.e., absolute volume) and brain scale (i.e., normalized volume), we have extensively analyzed our results using absolute volumes and relative volumes (normalized by total intracranial volume [TIV]). Moreover, to prevent the estimated models to be affected by wrongly processed images [Ducharme et al., 2016], we have used a demanding three stages quality control process. Finally, to be able to present a unified analysis of brain development and brain aging at the same time we considered hybrid models. Contrary to previous studies based on linear or low order polynomial models, we considered models enable to capture fast growth and complex degenerative processes. This is achieved by combining cumulative exponential function to model rapid growth with saturation resulting from maturation and low order polynomial function to model volume decrease caused by aging.

By putting all these elements together, we are able to show for the first time a global picture of brain trajectory across the entire lifespan. Our results suggest that most of the previous marked disagreements can be explained by the proposed analysis. Previous divergences seem mainly to result from restricted investigations over short periods of the entire life history. Indeed, as shown in the following, the analysis of subjects bellow 8 y of age is important to detect the maturation peak. Similarly, the analysis of subjects older than 80 y is necessary to observe the accelerated atrophy occurring at this age. We hope that the proposed unified analysis will help to reach a consensus on normal brain trajectory.

MATERIAL AND METHODS

Datasets

In this study, we used 3D T1-weight MRI obtained from nine freely available databases covering the entire lifespan. All the considered subjects are normal controls. The summary of used databases is detailed in Table I while details are provided latter in this section. The used images have been acquired on 1.5T and 3T over 103 sites. After quality control, 2,944 MRI were kept from the 3,296 considered subjects. The gender proportion of these selected subjects is 47% of female. The covered age starts from 9 months to

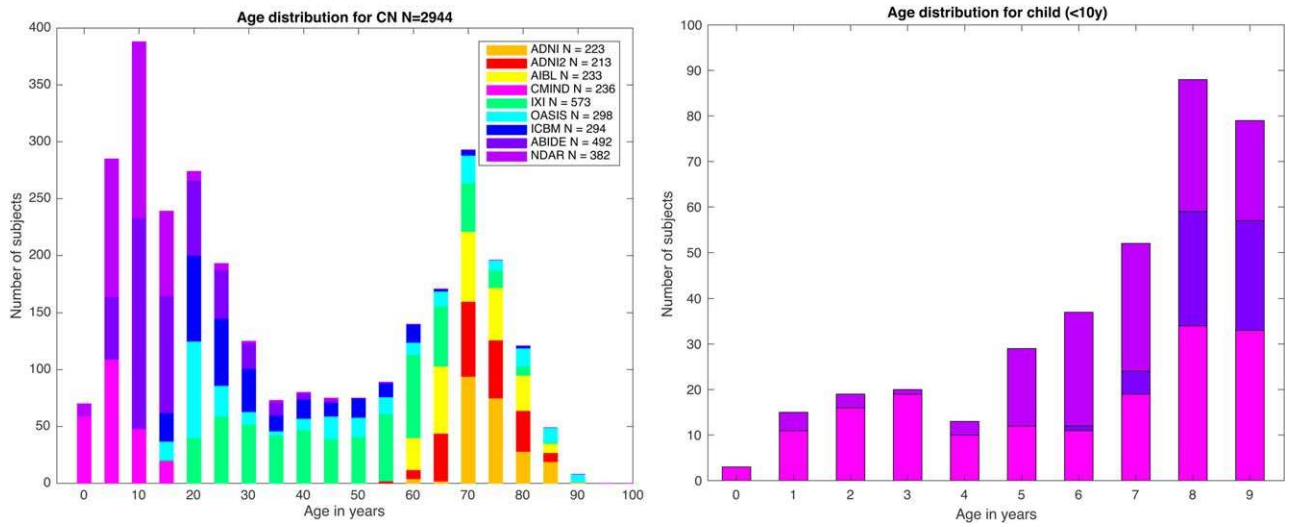

Figure 1.

Age distribution of the used MRI after the quality control. Left: Age distribution for all the considered subjects. Right: Age distribution for child younger than 10-y old. Legend indicates the database color and the number of image after quality control. [Color figure can be viewed at wileyonlinelibrary.com]

94 y, with an average age of 39.65 y and a standard deviation of 26.62.

Figure 1 shows the age distribution of the used subjects after quality. At least three different datasets are used for all the considered periods except for extreme ages (i.e., [0–4] y and [90–94] y) where only 2 datasets are available. Moreover, more than 50 subjects by 5-y interval are used at the exception of the last [90–94] interval.

In the following, more details about the different datasets used in this study are presented.

- C-MIND ($N = 266$, after QC $N = 236$): The images from the C-MIND dataset (https://research.cchmc.org/c-mind/) used in this study consist of 266 control subjects. All the images were acquired at the same site on a 3T scanner. The MRI are 3D T1-weighted MPRAGE high-resolution anatomical scan of the entire brain with spatial resolution of 1 mm^3 acquired using a 32 channel SENSE head-coil.
- NDAR ($N = 612$, after QC $N = 382$): The Database for Autism Research (NDAR) is a national database funded by NIH (https://ndar.nih.gov). This database included 13 different cohorts acquired on 1.5T MRI and 3T scanners. In our study, we used 415 images of control subjects from the NIHPD (http://www.bic.mni.mcgill.ca/nihpd/info/data_access.html) dataset and 197 images of control subjects from the Lab Study 19 of National Database for Autism Research. For the NIHPD, T1-weighted images were acquired at six different sites with 1.5 Tesla systems by General Electric (GE) and Siemens Medical Systems. The MRI are 3D T1-weighted spoiled gradient recalled (SPGR) echo sequence with following parameters: TR = 22–25 ms, TE = 10–11 ms, flip angle = 30°, FoV = 256 mm IS × 256 mm AP, matrix size = 256 × 256: 1 × 1 × 1 mm^3 voxels, 160–180 slices of sagittal orientation. The participants chosen from the Lab Study 19 of National Database for Autism Research (NDAR) were scanned using a 3T Siemens Tim Trio scanner at each site. The MRI are 3D MPRAGE sequence (voxel dimensions: 1.0 × 1.0 × 1.0 mm^3; image dimensions: 160 × 224 × 256, TE = 3.16 ms, TR = 2,400 ms).
- ABIDE ($N = 528$, after QC $N = 492$): The images from the Autism Brain Imaging Data Exchange (ABIDE) dataset (http://fcon_1000.projects.nitrc.org/indi/abide/) used in this study consist of 528 control subjects acquired at 20 different sites on 3T scanner. The MRI are T1-weight MPRAGE image and the details of acquisition, informed consent, and site-specific protocols are available on the website.
- ICBM ($N = 308$, after QC $N = 294$): The images from the International Consortium for Brain Mapping (ICBM) dataset (http://www.loni.usc.edu/ICBM/) used in this study consist of 308 normal subjects obtained through the LONI website. The MRI are T1-weighted MPRAGE (fast field echo, TR = 17 ms, TE = 10 ms, flip angle = 30°, 256 × 256 matrix, 1 mm^2 in plane resolution, 1 mm thick slices) acquired on a 1.5T Philips GyroScan imaging system (Philips Medical Systems, Best, The Netherlands).
- OASIS ($N = 315$, after QC $N = 298$): The images from the Open Access Series of Imaging Studies (OASIS) database (http://www.oasis-brains.org) used in this study consist of 315 control subjects. The MRI are T1-

weighted MPRAGE image (TR = 9.7 ms, TE = 4 ms, TI = 20 ms, flip angle = 10 degrees, slice thickness = 1.25 mm, matrix size = 256 × 256, voxel dimensions = 1 × 1 × 1.25 mm^3 resliced to 1 mm^3, averages = 1) acquired on a 1.5-T Vision scanner (Siemens, Erlangen, Germany).

- IXI ($N = 588$, after QC $N = 573$): The images from the Information eXtraction from Images (IXI) database (http://brain-development.org/ixi-dataset/) used in this study consist of 588 normal subjects. The MRI are T1weighted images collected at 3 sites with 1.5 and 3T scanners (FoV = 256 mm × 256 mm, matrix size = 0.9375 × 0.9375 × 1.2 mm^3).
- ADNI1 ($N = 228$, after QC $N = 223$): The images from the Alzheimer's Disease Neuroimaging Initiative (ADNI) database (http://adni.loni.usc.edu) used in this study consist of 228 control subjects from the 1.5T baseline collection. These images were acquired on 1.5T MR scanners at 60 different sites across the United States and Canada. A standardized MRI protocol to ensure cross-site comparability was used. Typical MRI are 3D sagittal MPRAGE (repetition time (TR): 2,400 ms, minimum full TE, inversion time (TI): 1,000 ms, flip angle: 8°, 24 cm field of view, and a 192 × 192 × 166 acquisition matrix in the *x*-, *y*-, and *z*-dimensions, yielding a voxel size of 1.25 × 1.25 × 1.2 mm^3, later reconstructed to get 1 mm^3 isotropic voxel resolution).
- ADNI2 ($N = 213$): The images from the ADNI2 database (second phase of the ADNI project) consist of 215 control subjects. Images were acquired on 3T MR scanners with the standardized ADNI-2 protocol, available online (www.loni.usc.edu). Typical MRI are T1-weighted 3D MPRAGE sequence (repetition time 2,300 ms, echo time 2.98 ms, flip angle 9°, field of view 256 mm, resolution 1.1 × 1.1 × 1.2 mm^3).
- AIBL ($N = 233$): The Australian Imaging, Biomarkers and Lifestyle (AIBL) database (http://www.aibl.csiro.au/) used in this study consists of 236 control subjects. The imaging protocol was defined to follow ADNI's guideline on the 3T scanner (http://adni.loni.ucla.edu/research/protocols/mri-protocols) and a custom MPRAGE sequence was used on the 1.5T scanner.

Image Processing

All the images were processed with volBrain online software pipeline (http://volbrain.upv.es). The volBrain system is a fully open access academic platform that we have developed during the last 5 y. This web-based platform offers to freely share our computational resources and our last image processing methods to all researchers over the world. Therefore, we used volBrain in this study since we perfectly know the software, the generated reports facilitate a fast first stage QC and we recently demonstrated its robustness and accuracy [Manjon and Coupe, 2016]. Recently, volBrain pipeline was compared with two well-known tools used on MR brain analysis (FSL and Freesurfer) showing significant improvements in terms of both accuracy and reproducibility for intrascanner and interscanner scan rescan acquisition [Manjon and Coupe, 2016]. Moreover, we knew that the system was able to process large dataset since volBrain provides automatic brain volumetry in less than 15 min (including the generation of a pdf volumetry report summarizing the volumetric results). Since its deployment (2 years ago), volBrain has processed online more than 37,000 MRI for more than 1,200 users.

The volBrain pipeline consists of a set of steps aimed to improve the quality of the MR images to analyze and to locate them in a common geometric and intensity space prior to perform segmentation at several anatomical levels [Manjon and Coupe, 2016]. In more details, volBrain pipeline includes the following preprocessing steps: (1) denoising using spatially adaptive nonlocal means [Manjon et al., 2010a], (2) rough inhomogeneity correction using N4 method [Tustison et al., 2010], (3) affine registration to MNI152 space using ANTS software [Avants et al., 2011], (4) SPM-based fine inhomogeneity correction [Ashburner and Friston, 2005], and (5) histogram-based intensity standardization. After the preprocessing, the intracranial cavity is segmented using NICE method [Manjon et al., 2014], tissue classification is performed using TMS method [Manjón et al.,, 2010b] and finally subcortical structures are estimated using an extended version of the nonlocal label fusion method [Coupe et al., 2011]. All the segmentation methods of volBrain use a library of 50 experts manually labelled cases (covering almost the whole lifespan) needed to perform the labeling process at different levels. More details can be found in [Manjon and Coupe, 2016].

Statistical Analysis

The statistical analysis was performed with Matlab© software. In order to determine the best general models for each structure, several models were tested from the simplest to the most complex on all the dataset (i.e., female and male at the same time). A model is kept as a potential candidate only when *F*-statistic based on ANOVA for model vs. constant model is significant ($P < 0.05$) and when all its coefficients are significant using *t*-statistic ($P < 0.05$). At the end of the selection procedure, we used the Bayesian information criterion (BIC) to select the best model among models being significant compared to constant model and having all coefficients significant. BIC provides a measure of the trade-off between bias and variance and thus select the model explaining most the data with minimum parameters. Afterwards, this general model type is applied on female and male separately to estimate gender specific models. At the end, to study

trajectory difference in terms of volume and shape between both female and male, β_iSex+ β_jSex.Age interactions are tested over the selected general model. All the reported parameters (t-statistic, F-statistic, BIC, and R^2) were internally estimated by Matlab© using default parameters. The following models were considered as potential candidates:

1. Linear model

$$\mathrm{Vol}=\beta_0+\beta_1\mathrm{Age}+\varepsilon$$

2. Quadratic model

$$\mathrm{Vol}=\beta_0+\beta_1\mathrm{Age}+\beta_2\mathrm{Age}^2+\varepsilon$$

3. Cubic model

$$\mathrm{Vol}=\beta_0+\beta_1\mathrm{Age}+\beta_2\mathrm{Age}^2+\beta_3\mathrm{Age}^3+\varepsilon$$

4. Linear hybrid model: exponential cumulative distribution for growth with linear model for aging

$$\mathrm{Vol}=\beta_4.\left(1-e^{-\mathrm{Age}/\beta_5}\right)+\beta_0+\beta_1\mathrm{Age}+\varepsilon$$

5. Quadratic hybrid model: exponential cumulative distribution for growth with quadratic model for aging

$$\mathrm{Vol}=\beta_4.\left(1-e^{-\mathrm{Age}/\beta_5}\right)+\beta_0+\beta_1\mathrm{Age}+\beta_2\mathrm{Age}^2+\varepsilon$$

6. Cubic hybrid model: exponential cumulative distribution for growth with cubic model for aging

$$\mathrm{Vol}=\beta_4.\left(1-e^{-\mathrm{Age}/\beta_5}\right)+\beta_0+\beta_1\mathrm{Age}+\beta_2\mathrm{Age}^2+\ \beta_3\mathrm{Age}^3+\varepsilon$$

In the literature, structure trajectories have been mainly modeled using low order polynomial function [see Walhovd et al., 2011 for review). However, to follow structure trajectories across the entire lifespan, we propose to consider hybrid models able to track rapid growth during childhood and to capture complex volume decrease from adulthood to elderly. In the past, fast growth modelling occurring during childhood has been achieved using Poisson curve [Lebel et al., 2012] or Gompertz-like function [Makropoulos et al., 2016]. Here, we propose to combine a cumulative exponential function in place of Gompertz-like function, and to combine it with low order polynomial function. At the end, our hybrid models can model fast growth process and complex volume decreases at the same time.

Quality Control

As recently shown, the quality control (QC) of image processing pipeline has a critical impact on trajectory results [Ducharme et al., 2016]. Therefore, in this study we decided to use a demanding multistage QC procedure for a careful selection of the involved subjects. First, a visual assessment of input image quality was done for all considered subjects. This assessment was performed by checking screen shots of one sagittal, one coronal and one axial slice in middle of the 3D volume. This step led to remove 219 subjects from the 3,296 considered subjects in our study (6.6%). Next, a visual assessment of the image processing quality for all remaining subjects was performed using volBrain reports (see an example of report here: http://volbrain.upv.es/example_report.pdf). This report provides screenshots of one sagittal, one coronal and one axial slice at middle of the 3D volume for each step of the processing pipeline. All these steps (full head coverage including cerebellum, registration to MNI space, TIV extraction, tissue classification, subcortical structure segmentation, etc.) were carefully checked. This step led to remove 83 subjects from our study (2.5%). Finally, a last control was performed by individually checking all outliers detected using estimated trajectories. A volume was considered as outlier when its value was higher/lower than 2 standard deviations of the estimated model. For each detected outlier, the segmentation map was opened and displayed over the MRI using a 3D viewer [Yushkevich et al., 2006]. A careful inspection was performed over the 3D volume. In case of segmentation failure, the subject was removed from the study. This last QC step led to remove 50 subjects (1.5%). Therefore, 2,944 of the 3,296 considered subjects were kept after our QC procedure.

RESULTS

Maturation and Aging of Brain Tissues

Global gray matter and white matter trajectories

At the global scale (i.e., absolute volumes), we observe an increase of WM volume until 30–40 y followed by a volume decrease (see Fig. 2). As it can be noticed, the WM growth at early ages is faster than the senescence at late ages. This is assessed by the selected hybrid model ($P < 0.001$) combining an exponential cumulative distribution model for growth and a cubic model for aging (see Table II). Conversely, although the same model is selected for GM ($P < 0.0001$), its trajectory is more complex. We can observe a 4-stage trajectory composed of a fast growth until 8–10 y followed by a fast decrease until 40 y, then a plateau and finally an accelerated aging-related decrease is visible around 80 y. At the brain scale, when using normalized volumes in % to the TIV (see Supporting Information Fig. 1), the main difference is found for the GM trajectory. Indeed, at this scale, we

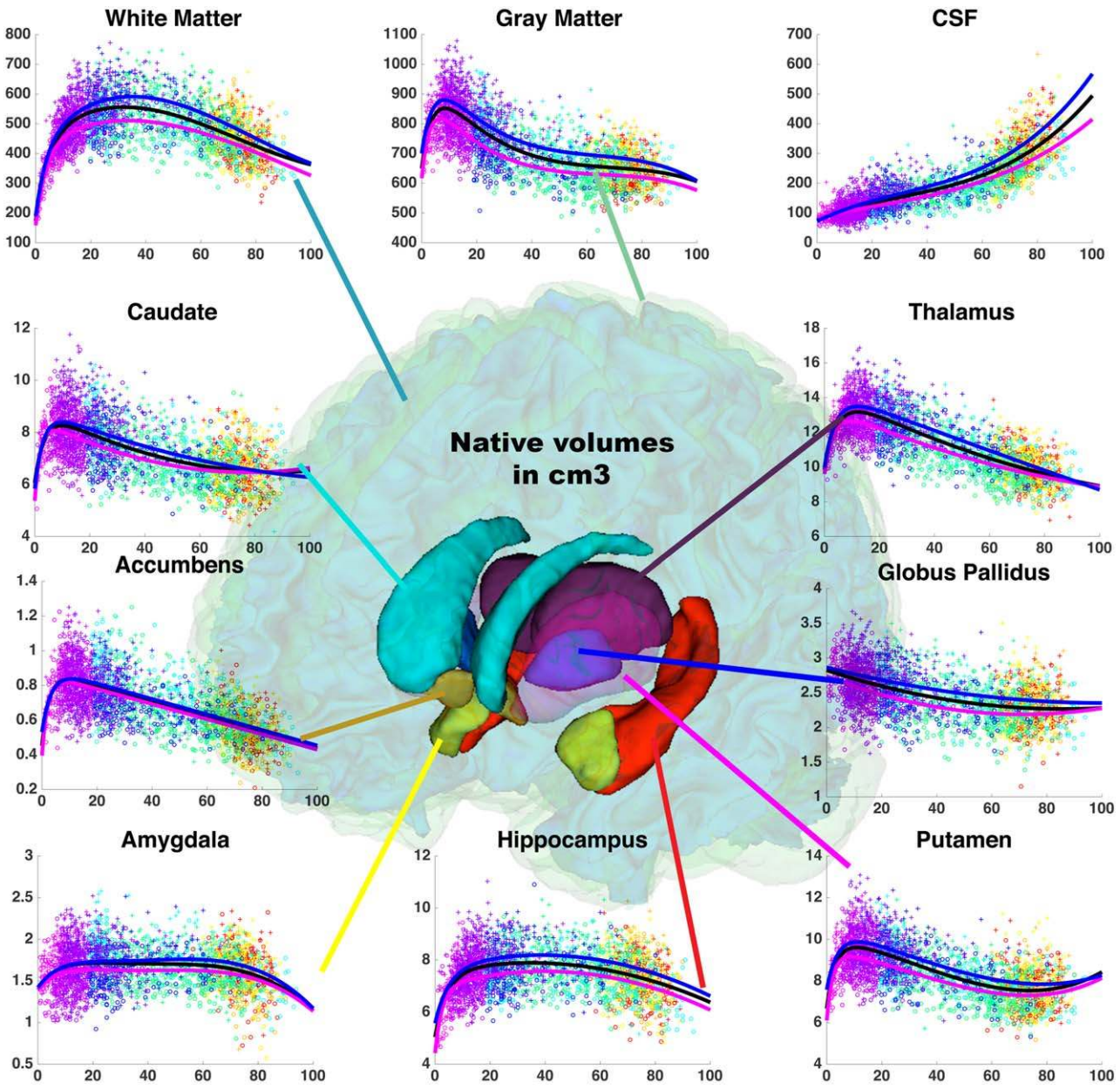

Figure 2.

Volume trajectories based on absolute volume in cm^3 for brain tissues and subcortical structures across the entire lifespan. These volume trajectories are estimated according to the age on 2,944 subjects from 9 months to 94 y. General model is in black, female model is in magenta and male model is in blue. Dots color represents the different datasets used in this study (see Fig. 1 for dataset color legend). [Color figure can be viewed at wileyonlinelibrary.com]

observe a decrease of GM all along the lifespan (see Fig. 3) following a cubic model ($P < 0.0001$) (see Table III). The decrease of normalized volumes also follows a complex shape with three stages composed of a rapid decrease from 0 to 20 y, a plateau from 40 to 80 y and a rapid decrease after 80 y. It is interesting to note that despite the normalization, the WM growth remains very fast at the brain scale for early age with a hybrid model using an exponential cumulative distribution model for growth. Finally, at global and brain scales, we observe that WM have almost an inverted U-shape model although an asymmetry exists with a faster volume

TABLE II. Results of model analysis for absolute volumes

Absolute volume	Selected Model	*F*-Statistic	R^2	Model vs. constant model *P*-value of the *F*-statistic based on ANOVA	Gender interaction *P*-value of the *t*-statistic on the coefficient	Age × gender interaction *P*-value of the *t*-statistic on the coefficient
White Matter						
Global	Hybrid third order	472	0.39	$P < 0.0001$	$\mathbf{P \leq 0.0001}$	$P = 0.77$
Male		291	0.43	$P < 0.0001$		
Female		230	0.40	$P < 0.0001$		
Gray Matter						
Global	Hybrid third order	938	0.56	$P < 0.0001$	$\mathbf{P \leq 0.0001}$	$P = 0.19$
Male		536	0.45	$P < 0.0001$		
Female		529	0.61	$P < 0.0001$		
CSF						
Global	third order	2,770	0.74	$P < 0.0001$	$P = 0.90$	$\mathbf{P \leq 0.0001}$
Male		813	0.81	$P < 0.0001$		
Female		1,380	0.75	$P < 0.0001$		
Caudate						
Global	Hybrid third order	590	0.37	$P < 0.0001$	$\mathbf{P = 0.006}$	$P = 0.25$
Male		307	0.37	$P < 0.0001$		
Female		255	0.36	$P < 0.0001$		
Putamen						
Global	Hybrid third order	593	0.45	$P < 0.0001$	$\mathbf{P \leq 0.0001}$	$P = 0.28$
Male		315	0.45	$P < 0.0001$		
Female		262	0.43	$P < 0.0001$		
Thalamus						
Global	Hybrid second order	1,730	0.64	$P < 0.0001$	$\mathbf{P \leq 0.0001}$	$P = 0.11$
Male		977	0.65	$P < 0.0001$		
Female		840	0.65	$P < 0.0001$		
Globus Pallidus						
Global	Second order	494	0.25	$P < 0.0001$	$\mathbf{P \leq 0.001}$	$P = 0.78$
Male		203	0.21	$P < 0.0001$		
Female		281	0.29	$P < 0.0001$		
Hippocampus						
Global	Hybrid second order	177	0.15	$P < 0.0001$	$\mathbf{P = 0.001}$	$P = 0.99$
Male		85.3	0.14	$P < 0.0001$		
Female		90.2	0.16	$P < 0.0001$		
Amygdala						
Global	Hybrid third order	46.3	0.06	$P < 0.0001$	$\mathbf{P = 0.045}$	$P = 0.90$
Male		23.3	0.06	$P < 0.0001$		
Female		24.0	0.05	$P < 0.0001$		
Accumbens						
Global	Hybrid first order	1,250	0.46	$P < 0.0001$	$P = 0.37$	$P = 0.97$
Male		598	0.43	$P < 0.0001$		
Female		592	0.46	$P < 0.0001$		

increase related to maturation than volume decrease caused by aging.

Cortical and subcortical gray matter trajectories

To study trajectory differences between cortical and deep gray matter, we performed complementary analyses (see Supporting Information Table 1). First, we estimated the deep GM volume by adding the GM volume of the considered deep structures (i.e., caudate, thalamus, accumbens, globus pallidus, putamen, hippocampus, and amygdala). The cortical GM was estimated as the global GM volume (as used in the paper) minus the deep GM volume. Figure 4 shows the estimated trajectories using absolute volume and normalized volume in % of TIV. At the global scale, we can observe that after their maturation peaks, deep and cortical GM volume decreases. However, deep GM volume decreases with almost a constant rate while cortical GM volume follows a more complex trajectory similar to the four-stage pattern already described for global GM. Similarly, at the brain scale, while the cortical GM follows the 3 stages detailed for global GM, the deep GM follows an almost linear decrease all along the lifespan with an accelerated atrophy after 80 y.

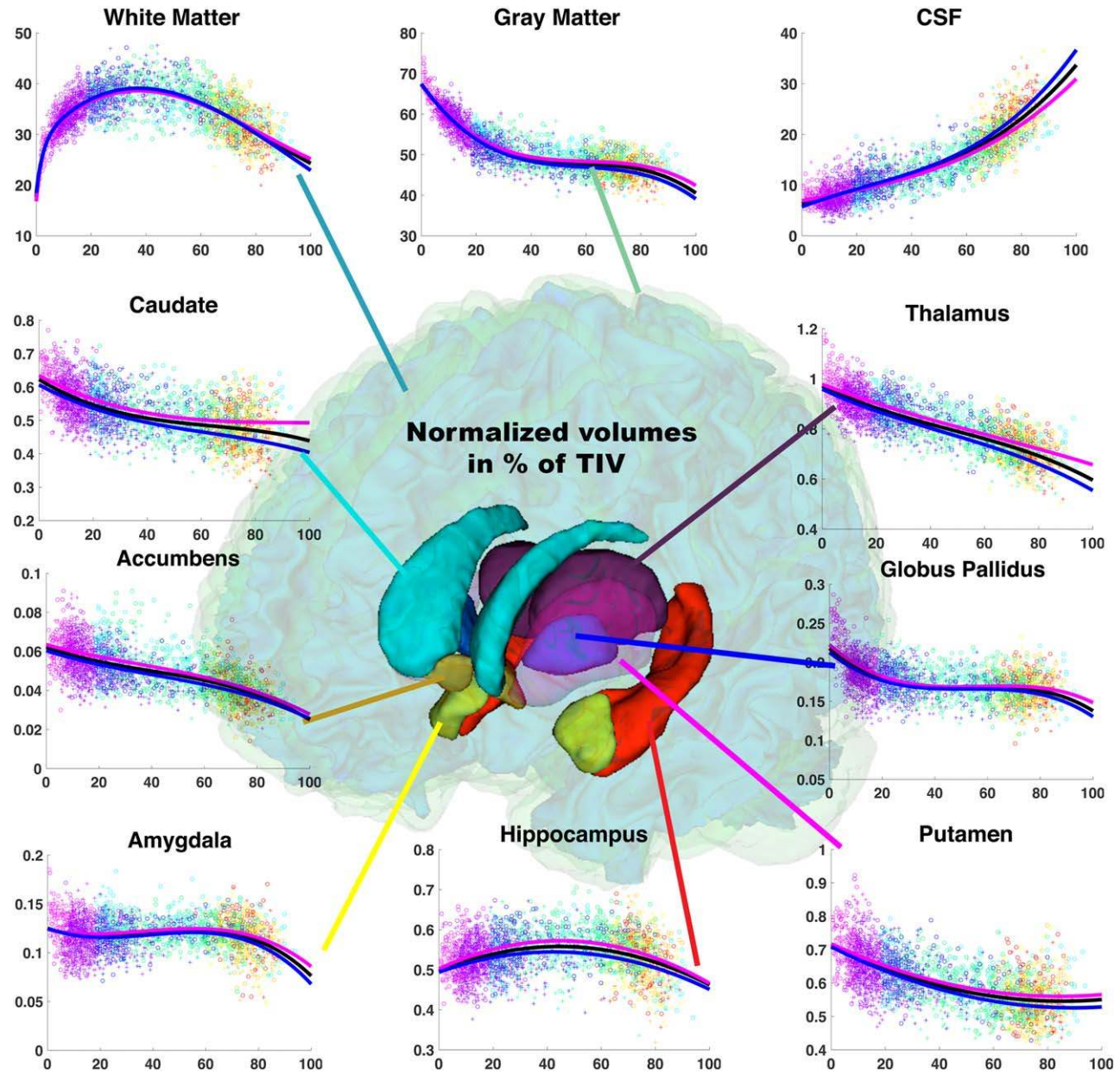

Figure 3.

Trajectories based on relative volumes (% total intracranial volume) for brain tissues and subcortical structures across the entire lifespan. These volume trajectories are estimated according to the age on 2,944 subjects from 9 months to 94 y. General model is in black, female model is in magenta and male model is in blue. Dots color represents the different datasets used in this study (see Fig. 1 for dataset color legend). [Color figure can be viewed at wileyonlinelibrary.com]

Cerebrum and cerebellum trajectories

Finally, we investigated cerebrum and cerebellum trajectories separately. At global scale, selected models for cerebrum and cerebellum are the same and they are similar to the models selected for global GM and WM (see Supporting Information Tables 2 and 3). Moreover, gender differences were found for cerebrum and cerebellum when using absolute volumes. Visually, both structures follow similar trajectories (see Figs. 5 and 6). However, some differences can be observed. First, the cerebellum has a shorter GM volume decrease after maturation peak. In addition, the magnitude of GM and WM increase during

TABLE III. Results of model analysis for relative volumes normalized by TIV

Relative volume in % of TIV	Selected Model	*F*-Statistic	R^2	Model vs. constant model *P*-value of the *F*-statistic based on ANOVA	Gender interaction *P*-value of the *t*-statistic on the coefficient	Age × gender interaction *P*-value of the *t*-statistic on the coefficient
White Matter						
Global	Hybrid third	837	0.53	$P < 0.0001$	$P = 0.32$	$P = 0.41$
Male	order	466	0.54	$P < 0.0001$		
Female		369	0.52	$P < 0.0001$		
Gray Matter						
Global	third order	4,030	0.80	$P < 0.0001$	$P = 0.80$	$P = 0.06$
Male		2,380	0.82	$P < 0.0001$		
Female		1,920	0.81	$P < 0.0001$		
CSF						
Global	third order	4,450	0.82	$P < 0.0001$	$P = 0.25$	**$P = 0.003$**
Male		2,910	0.85	$P < 0.0001$		
Female		1,880	0.80	$P < 0.0001$		
Caudate						
Global	third order	569	0.37	$P < 0.0001$	**$P = 0.05$**	$P = 0.31$
Male		307	0.44	$P < 0.0001$		
Female		282	0.38	$P < 0.0001$		
Putamen						
Global	second order	1,110	0.43	$P < 0.0001$	$P = 0.37$	$P = 0.37$
Male		743	0.49	$P < 0.0001$		
Female		471	0.41	$P < 0.0001$		
Thalamus						
Global	third order	2,180	0.69	$P < 0.0001$	**$P = 0.05$**	$P = 0.20$
Male		1,540	0.75	$P < 0.0001$		
Female		1,050	0.70	$P < 0.0001$		
Globus Pallidus						
Global	third order	398	0.29	$P < 0.0001$	$P = 0.12$	$P = 0.83$
Male		205	0.28	$P < 0.0001$		
Female		215	0.32	$P < 0.0001$		
Hippocampus						
Global	second order	140	0.09	$P < 0.0001$	$P = 0.07$	$P = 0.67$
Male		60	0.07	$P < 0.0001$		
Female		94.9	0.12	$P < 0.0001$		
Amygdala						
Global	third order	47.2	0.05	$P < 0.0001$	$P = 0.56$	$P = 0.50$
Male		29.9	0.05	$P < 0.0001$		
Female		19.5	0.04	$P < 0.0001$		
Accumbens						
Global	third order	725	0.42	$P < 0.0001$	**$P = 0.02$**	$P = 0.65$
Male		427	0.45	$P < 0.0001$		
Female		368	0.44	$P < 0.0001$		

maturation is smaller for the cerebellum than for cerebrum. Finally, the cerebellum has a less pronounced WM decrease after 80 y and has a reduced atrophy rate over this period. At the brain scale, selected models are different between cerebrum WM and cerebellum WM. The hybrid model selected for WM cerebrum indicates a faster volume increase for this structure compared to WM cerebellum. The faster maturation during childhood of WM cerebrum is also visible on Figures 5 and 6. The three-stage trajectory obtained for global GM is observed for cerebellum GM and cerebrum GM. However, the plateau occurring at adulthood appears earlier for cerebellum than for cerebrum. Finally, the atrophy rate of normalized cerebrum volume is faster than cerebellum one.

Deep Gray Matter Structure Trajectories

Thalamus, accumbens, caudate, putamen, and globus pallidus trajectories

At global scale, we observe that thalamus, accumbens, caudate and putamen follow similar trajectories with fast growth until 10–12 y followed by a volume decrease. All selected hybrid models combine an exponential cumulative distribution for growth followed by low polynomial order for volume loss during aging, cubic for caudate ($P < 0.0001$) and putamen ($P < 0.0001$), quadratic for thalamus ($P < 0.0001$), and linear for accumbens ($P < 0.0001$) (see Table II). Conversely, globus pallidus volume decreases from birth all

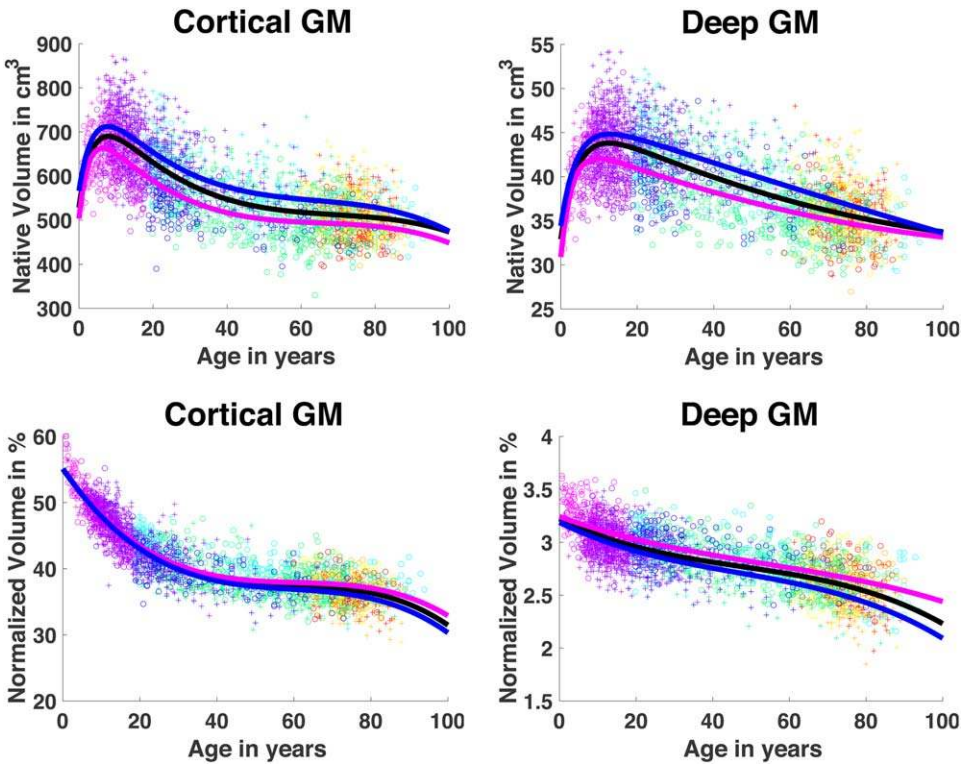

Figure 4.

Trajectory of the cortical and deep GM volumes in cm^3 and % of TIV across the entire lifespan. These volume trajectories are estimated according to the age on 2,944 subjects from 9 months to 94 y. General model is in black, female model is in magenta and male model is in blue. Dots color represents the different datasets used in this study (see Fig. 1 for dataset color legend). [Color figure can be viewed at wileyonlinelibrary.com]

along lifespan (quadratic model with $P < 0.0001$). Unexpected slight increases of caudate and putamen volumes are visible after 80 y. At the brain scale, we can see that thalamus, accumbens, caudate, putamen, and globus pallidus show a volume decrease across the entire lifespan. First, thalamus and accumbens exhibit almost monotonous decrease although cubic models have been selected (both with $P < 0.0001$). Second, caudate and putamen present similar slowdown decreases after 50 y. The similar trajectories of the caudate and putamen are consistent with their shared nature as dorsal striatal structures [Paxinos and Mai, 2004]. The model selected for these structures is cubic for caudate ($P < 0.0001$) and quadratic for putamen ($P < 0.0001$; see Table III). Finally, globus pallidus follows a cubic model ($P < 0.0001$) showing a fast decrease between 1 y and 30 y, followed by a plateau between 30 y and 80 y and then by an accelerated atrophy after 80 y.

Amygdala and hippocampus trajectories

At the global scale, amygdala volume shows a slight increase until 18 y–20 y followed by a long plateau that ends around 70 y, followed by an age-related atrophy. The selected hybrid model combines a volume increase following an exponential cumulative distribution and a volume decrease following cubic model ($P < 0.0001$). The hippocampus trajectory presents a fast volume increase until 8 y–10 y followed by a slow volume increase until 40 y–50 y before an atrophic period. Here, the selected hybrid model mixes a volume increase following an exponential cumulative distribution and then an inverted U-shape volume decrease ($P < 0.0001$). At the brain scale, amygdala volume trajectory follows a cubic model ($P < 0.0001$) with a plateau until 70 y followed by an atrophy. This result seems to indicate that absolute increase of amygdala volume during childhood is mainly related to brain growth. Moreover, using relative volume, hippocampus exhibit a very specific inverted U-shape trajectory compared to other analyzed subcortical structures. In our study, the hippocampus is the only structure showing volume increase until the middle period of human life. To better investigate this point, we performed a complementary analysis between 18 y and 70 y. We found that the impact of age on absolute HC volume is significant ($P < 0.0001$) and that the selected model is an inverted U-shape trajectory over this restricted period. According to our results, the hippocampal maturation stops around 50 y.

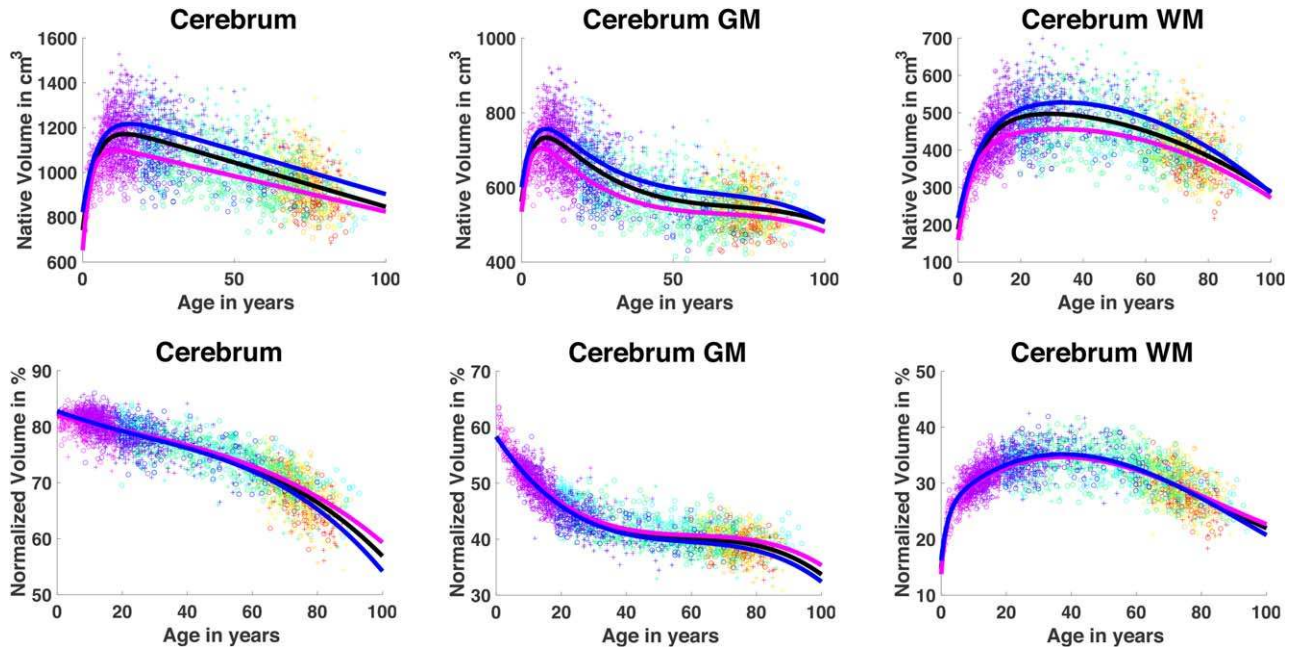

Figure 5.

Trajectory of the cerebrum, cerebrum GM and cerebrum CM volumes in cm^3 and % of TIV across the entire lifespan. These volume trajectories are estimated according to the age on 2,944 subjects from 9 months to 94 y. General model is in black, female model is in magenta and male model is in blue. Dots color represents the different datasets used in this study (see Fig. 1 for dataset color legend). [Color figure can be viewed at wileyonlinelibrary.com]

Sexual Dimorphism

At the global scale, we observe that males have bigger volumes than females for all considered structures (sex interaction with $P < 0.0001$, see Table II) with the exception of accumbens. Finally, increased atrophy rates for males after 80 y is assessed by CSF trajectory, which is the only brain compartment showing significant age × sex ($P < 0.0001$) over the entire lifespan using the considered model. At the brain scale, almost all gender volume differences vanish, except in favor of females for caudate ($P = 0.05$) and thalamus ($P = 0.05$) with marginal significance, and for accumbens ($P = 0.02$) (see Table III). Visually, we can observe bigger relative volume for female hippocampus almost significant ($P = 0.07$; see Table III and Fig. 3). Finally, for global GM, caudate, thalamus, globus pallidus and amygdala, trajectories of females seem to indicate a better resistance to the accelerated age-related atrophy occurring after 80 y. To investigate this point, we studied sex and sex × age interaction using all subjects with age > 70 y (i.e., 637 subjects composed of 292 males and 345 females). Models estimated using all the subjects (see Table II) are applied over this considered restricted period to evaluate sex and sex × age interactions. We found that using normalized volumes, almost all studied structures show significant sex and sex × age interaction after 70 y with the exception of WM and amygdala (see Table IV).

DISCUSSION

One of the main questions related to brain tissue properties deals with gray and white matter development/maturation and age-related gray and white matter atrophy. Knowing when brain tissues stop to mature and when they start to degenerate are key questions in neurology [Sowell et al., 2003]. In the past, both questions have been mainly treated separately in the literature, preventing us to get a global picture of these join phenomena. Moreover, discrepancies between used volumetric measurements (absolute or relative) made difficult to reach a consensus on crucial questions about synaptogenesis and synaptic pruning or myelination and aging.

Towards a Consensus?

Marked discrepancies exist in the literature about the best fitting models to describe brain trajectories either in pediatric phase [Ducharme et al., 2016] or adulthood [Fjell et al., 2013]. In our study, hybrid models mixing exponential cumulative distribution growth with low order

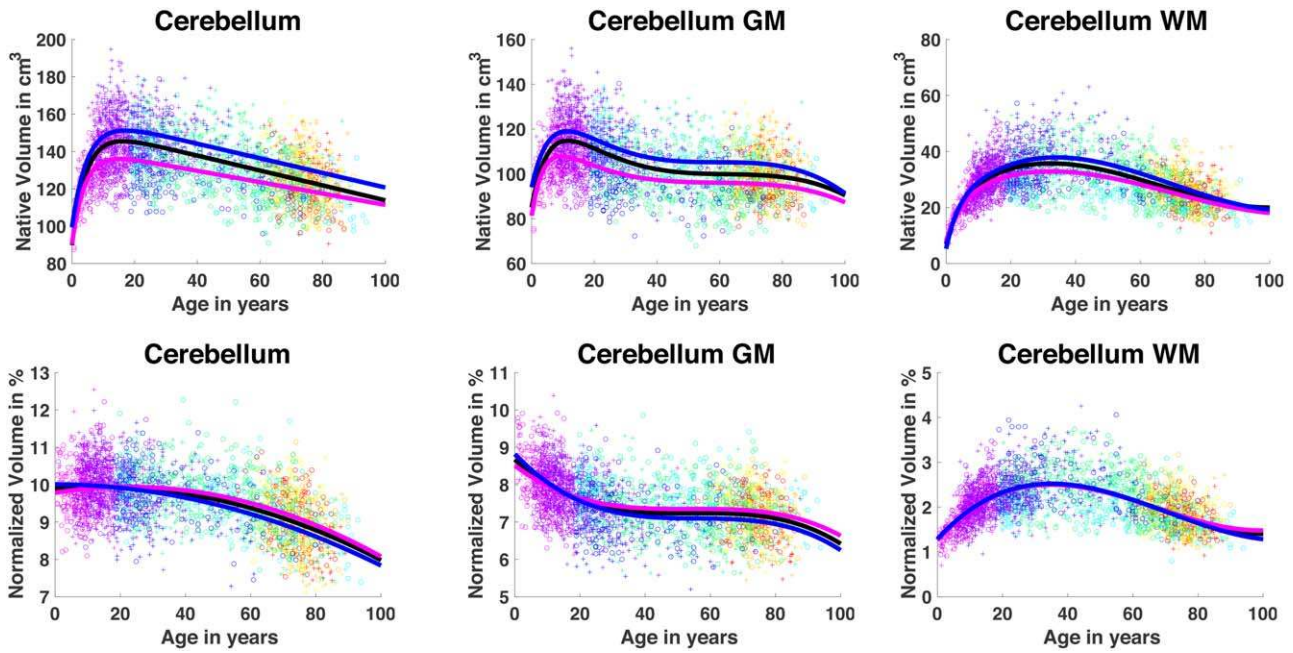

Figure 6.

Trajectory of the cerebellum, cerebellum GM and cerebellum WM volumes in cm^3 and % of TIV across the entire lifespan. These volume trajectories are estimated according to the age on 2,944 subjects from 9 months to 94 y. General model is in black, female model is in magenta and male model is in blue. Dots color represents the different datasets used in this study (see Fig. 1 for dataset color legend). [Color figure can be viewed at wileyonlinelibrary.com]

polynomial senescence were selected for 8/10 of the investigated brain regions when absolute volumes are used. Moreover, the absolute global GM volume follows a complex trajectory with four phases: (1) rapid increase from 0 to 8–10 y, (2) rapid decrease until 40, (3) a plateau from 40 to 80 y, and (4) a rapid decrease after 80 y. Conversely, low order polynomial models better fit when volumes normalized by TIV are used, except for WM (see Tables II and III). When global growth effect is corrected, normalized global GM volumes decrease all over lifespan and follow a complex shape with three phases: (1) a rapid decrease from 0 to 20 y, (2) a plateau from 40 to 80 y, and (3) a rapid decrease after 80 y. This decline of the normalized global GM volume is consistent with the well-known fact that most of the neurogenesis is a prenatal phenomenon [Stiles and Jernigan, 2010]. In contrast, WM presents a shape close to the usually described inverted U-shape [Walhovd et al., 2011] that persists after controlling for head size. This result indicates that during the early phase of brain development WM expansion exceeds general growth. The fast simultaneous WM maturation and GM decrease at brain scale from childhood to adolescence are consistent with brain myelination period and cortical thinning process previously observed ex vivo [Huttenlocher and Dabholkar, 1997]. When considering cortical GM and deep GM separately, they exhibit a different pattern at both global and brain scales. At brain scale, deep GM shows almost a linear decrease while cortical GM trajectory follows the three identified stages for the global GM (see Fig. 4). The steeper decrease of normalized volume for cortical GM in the 0–20 y period (compared to the almost linear dynamics of the deep GM) is probably due to the very high pruning rate of the exuberant connectivity generated in the cerebral cortex [Stiles and Jernigan, 2010] or is due to myelination of nearby subcortical WM fibers [Jernigan et al., 2011].

One of the most marked discrepancy in the literature is about the cortical GM trajectory over childhood [Walhovd et al., 2016]. First studies reported an increase with maturation peak in early school age [Giedd et al., 1999; Lenroot et al., 2007; Raznahan et al., 2011]. However, mainly monotonic decrease from early childhood have been recently published [Aubert-Broche et al., 2013; Brain Development Cooperative Group, 2012; Ducharme et al., 2016; Mills et al., 2016; Ostby et al., 2009]. The first factor that could explain this pronounced divergence is the used volume measurement. In this study, we showed that absolute GM volume follows a 4-stage trajectory with a maturation peak while normalized GM volume follows a three-stage trajectory exhibiting a decrease all along the lifespan. Therefore, our results are in line with [Giedd et al., 1999; Groeschel et al., 2010; Raznahan et al., 2011; Shaw et al., 2008] using

TABLE IV. Results on normalized volumes for 637 subjects older than 70 y

	Relative volume in % of TIV	
	Gender interaction P-value of the t-statistic on the coefficient	Age × gender interaction P-value of the t-statistic on the coefficient
White Matter	$P = 0.14$	$P = 0.14$
Gray Matter	$\mathbf{P = 0.0002}$	$\mathbf{P = 0.0001}$
CSF	$\mathbf{P = 0.002}$	$\mathbf{P = 0.0015}$
Caudate	$\mathbf{P = 0.03}$	$\mathbf{P = 0.01}$
Putamen	$\mathbf{P = 0.0001}$	$\mathbf{P \leq 0.0001}$
Thalamus	$\mathbf{P = 0.001}$	$\mathbf{P = 0.0005}$
Globus Pallidus	$\mathbf{P = 0.0002}$	$\mathbf{P = 0.0001}$
Hippocampus	$\mathbf{P = 0.03}$	$\mathbf{P = 0.04}$
Amygdala	$P = 0.38$	$P = 0.34$
Accumbens	$\mathbf{p = 0.03}$	$\mathbf{P = 0.02}$

The result for absolute TIV over this restricted period is $P = 0.50$ for gender interaction and $P = 0.35$ for Age × gender interaction.

absolute measurement and are consistent with [Mills et al., 2016; Ostby et al., 2009] using normalized measurement. However, several studies reported monotonic decrease using absolute cortical GM volume over childhood [Aubert-Broche et al., 2013; Brain Development Cooperative Group, 2012; Ducharme et al., 2016; Mills et al., 2016; Sowell et al., 2003; Walhovd et al., 2016]. This result is in contradiction with studies dedicated to newborn period that report an increase of absolute GM over the first months of life [Groeschel et al., 2010; Holland et al., 2014; Makropoulos et al., 2016]. The fact that several studies did not detect GM maturation peak using absolute measurements seems to be related to two main factors, the lack of subjects younger than 5 y and the use of low order polynomial models. Indeed, most of the studies presenting monotonic decrease did not include subjects younger than 4 y making difficult the detection of GM volume increase over the first years of life. Moreover, this implies that the model fitting was mainly driven by subjects with already mature brains [Aubert-Broche et al., 2013; Brain Development Cooperative Group, 2012; Ducharme et al., 2016; Mills et al., 2016; Sowell et al., 2003; Walhovd et al., 2016]. In addition to this potential issue on the used age range, most of these studies were using linear, quadratic or cubic models. Low order polynomial models are not well-designed to capture complex shape such as fast growth with saturation before nonlinear decrease. In our study, we tried to address these two limitations by using subjects younger than 4-y old and by considering hybrid models able to handle complex brain change occurring during the first years of life. Finally, it is interesting to note that our results are in line with another study presenting GM trajectory from infancy to young adulthood based on nonlinear piecewise polynomial model [Groeschel et al., 2010].

Deep GM structures are the focus of a great interest due to their important role in various neurodegenerative diseases, and thus have been intensively studied in the past [Fjell et al., 2013]. Nonlinear trajectories of these structures have been previously described for adulthood [Fjell et al., 2013; Ziegler et al., 2012]. More recently, studies taking advantage of the "BigData sharing" in neuroscience started to analyze subcortical structure volumes from 20 y up to advanced ages to define normative values for adult lifespan [Potvin et al., 2016]. However, the limited age range of these studies made impossible to estimate full lifespan models. In this study, we have addressed this important problem by considering subjects covering the entire lifespan. Moreover, we extensively analyzed structure trajectories using both absolute and normalized volumes. Therefore, our results present at the same time the structure maturation peaks occurring during childhood based on absolute volumes and the accelerated atrophy related to aging occurring after 80 y obtained using normalized volumes. In addition, when deep GM structures are considered at the brain scale, their trajectories present a similar global decrease all along life, except for the medio-temporal regions with a late decrease for amygdala (after 70-y old) and an inverted U-shape for hippocampus. Moreover, an unexpected slight increase of caudate and putamen absolute volumes is visible after 80 y. Such observations have been already reported and questioned in several studies [Fjell et al., 2013; Potvin et al., 2016; Walhovd et al., 2011]. Different hypotheses have been proposed such as bias related to survival of subjects with bigger structures, cohort effect, image artifact related to aging or a real phenomenon [Potvin et al., 2016]. In our opinion, such volume increases at late ages can be also related to the use of global parametric model with less samples for very old subjects.

The understanding of the amygdalo-hippocampal complex is important in neurology since it is related to crucial tasks such as memory, spatial navigation, or emotional behavior. Moreover, hippocampus has been largely studied due to its use as an early biomarker in several neurodegenerative diseases such as Alzheimer's disease [Fox et al., 1996; Jack et al., 1997] but also because it is the main

location of adult neurogenesis [Eriksson et al., 1998; van Praag et al., 2002]. Noteworthy, while amygdala and hippocampus are often associated due to their respective contribution to the limbic system, it appears that they present different trajectories. This fact has been previously reported in recent studies [Fjell et al., 2013; Pfefferbaum et al., 2013; Potvin et al., 2016; Ziegler et al., 2012]. The long maturation period of the hippocampus may be related to the adult neurogenesis. In fact, it has been shown that neurogenesis in the human hippocampus is substantial until at least the fifth decade of life [Spalding et al., 2013], a finding consistent with our analysis. In contrast to the hippocampus, early maturation of the amygdala is consistent with its known function in emotional learning, which allows individuals to avoid aversive events and pursue rewarding experiences [Phelps and LeDoux, 2005]. Accordingly, the amygdala in humans has been shown to be functional early in life [Tottenham and Sheridan, 2009]. Our results on amygdala are in accordance with most of the previous studies highlighting a minor effect of aging over adulthood [Walhovd et al., 2011].

Another important question about brain maturation and aging is related to sexual dimorphism. In the past, this question has been studied mainly over childhood development [Aubert-Broche et al., 2013; Brain Development Cooperative Group, 2012; Giedd and Rapoport, 2010] or during adolescence [Hu et al., 2013; Lenroot and Giedd, 2010; Lenroot et al., 2007; Ostby et al., 2009]. As previously mentioned, studies on different limited time periods, using nonharmonized tools and different volumetric measurements prevented reaching a consensus. In our study, when using absolute volume, we found that brain structure maturation peaks occur before for female than for male (between 1 y and 3 y earlier). These earlier peaks in females in the maturational phase have been previously described [Giedd and Rapoport, 2010] and were mainly explained by sex differences in growth. We also found a difference around 10–12% of brain size between sexes as previously reported by in vivo or postmortem studies [Brain Development Cooperative Group, 2012; Lenroot and Giedd, 2010]. Conversely, when the impact of brain size is compensated for, both sexes exhibit more similar trajectories. Only the normalized volume of nucleus accumbens presents a marked sexual dimorphism. This region is a key structure in the neural circuitry of addiction, a phenomenon well-known to show sex differences [Becker and Hu, 2008]. However, sexual dimorphism of the accumbens volume in humans has not been (to our knowledge) described before. In rats, a higher density of dendritic spines has been shown in females [Forlano and Woolley, 2010]. If a similar sex difference would exist in humans, it would be so subtle that only very large experimental samples would reveal it, as it is the case in the present study. Finally, we found that for several structures males are more impacted by aging than females especially after 70 y. The fact that women may be less vulnerable to age-related atrophy has been previously reported [Carne et al., 2006; Coffey et al., 1998; Gur et al., 1991]. This phenomenon may be related to the protective effect of estrogens and progesterone [Green and Simpkins, 2000] or related to the fact that women present fewer risk factors (hypertension, tobacco, alcohol consummation, etc.).

Limitations

In our opinion, one of the strengths of our study is to use multiple datasets to be able to cover the entire lifespan. However, this point can be also viewed as a weakness since the use of multiple datasets may introduce bias. Indeed, pooling databases having different age ranges could lead to find artificial differences. It has to be noted that we limited this aspect by using at least two different overlapping databases for each 5 y intervals. Moreover, the preprocessing pipeline of volBrain has been designed to limit the impact of acquisition protocol by proposing advanced denoising filter and tissue-based intensity normalization. Therefore, after preprocessing, images are better homogenized in terms of signal-to-noise ratio and tissue contrast limiting the impact of using different acquisition protocols and scanners. In addition, during our QC all images with motion and ghosting artifacts were removed as well as the image having high anisotropic voxel resolution. Finally, several studies showed that age-related volume differences are consistent between datasets when using the same analysis tool [Fjell et al., 2009; Mills et al., 2016; Walhovd et al., 2011]. Moreover, recent papers based on a large scale study over adulthood [Potvin et al., 2016, 2017] showed that the impact of MRI scanner manufacturer and magnetic strength is negligible compared to impact of age of the structure trajectories.

After our quality control step, no images of subjects younger than 9 months remained. Therefore, the newborn period is not well covered by our samples and thus results obtained before 9 months of life may be inaccurate. Few studies have been published on brain structure trajectory for this since the acquisition is difficult and the image analysis is very challenging due to low contrast before 6 months and fast myelination progression during the first 2 y of life [Gilmore et al., 2007, 2012; Groeschel et al., 2010; Holland et al., 2014; Makropoulos et al., 2016]. However, specific tools have been proposed to analyze the newborn life period [Makropoulos et al., 2014; Wang et al., 2014]. Nevertheless, up to now, there is no large period lifespan study integrating newborn period with childhood, adolescence, adulthood and elderly.

Here, we described different lifespan trajectories for deep versus cortical structures. Previous studies described heterogeneous trajectories for different parts of the cortex over restricted periods [Fjell et al., 2009; Pfefferbaum et al., 2013; Potvin et al., 2017; Sowell et al., 2003; Walhovd et al., 2016]. Therefore, we plan to investigate trajectory based on

cortex parcellation over the entire lifespan in a further study.

Finally, we used cross-sectional analysis to study brain trajectory over the entire lifespan. Using cross-sectional data to analyze a dynamic process can be suboptimal. However, some evidences show that cross-sectional and longitudinal samples produce similar age-related patterns [Fjell et al., 2013]. Moreover, the reported lack of consensus is also observed among different longitudinal studies. For instance, the volume of cortical gray matter is highest in childhood according to some longitudinal studies [Mills et al., 2016], but peaks at puberty according to others [Lenroot et al., 2007]. Therefore, the longitudinal or cross-sectional nature of the data is another factor introducing variability but it is not the unique factor explaining the different results reported in the literature. It is interesting to note that most of the trajectories obtained in our cross-sectional study are in accordance with previous longitudinal studies. First, for childhood, maturation peak between 8 y and 10 y for absolute cortical GM volume and earlier peak for females have been reported using longitudinal data [Giedd et al., 1999; Raznahan et al., 2011]. Moreover, for adolescence, an increase of the absolute WM volume and a decrease of absolute GM volume between 10 y and 20 y have been observed in previous longitudinal studies [Aubert-Broche et al., 2013; Giedd et al., 1999; Mills et al., 2016]. Finally, for adulthood, our results on normalized subcortical structures volume are highly consistent with results presented in the longitudinal study published by Pfefferbaum et al. [2013]. Nevertheless, we think that in a further work, a mixed cross-sectional/longitudinal study [Giedd et al., 1999] could be done since some of the used datasets contain longitudinal data.

CONCLUSION

We have presented an MRI volumetric brain analysis study covering the entire lifespan based on a very large number of subjects. In this study, we have dealt with main limitations of previous studies to offer a comprehensive analysis of maturation and aging effects at different brain tissues and structures. Absolute and relative measurements have been used to get a complete picture of the brain state at different development stages for both genders. Moreover, optimized models have been used to robustly characterize volume evolution of the different tissues and structures. The results of this study are very helpful to integrate several previous studies covering partial age ranges into a common framework. This enables a better understanding of the observed phenomena. Moreover, the use of the estimated models as normative values can be of inestimable help when analyzing the state of new subjects. Furthermore, disease specific estimated models can be directly compared to the normal models estimated in this study without needing to acquire and analyze a control group. We will include these models in our open access web platform volBrain to provide normality bounds based on the appropriate sex and age for the analysis of new cases. We hope that the online availability of the volBrain online service in combination with the presented models will help our understanding of both normal and pathological human brain.

ACKNOWLEDGMENTS

Moreover, this work is based on multiple samples. We wish to thank all investigators of these projects who collected these datasets and made them freely accessible.

The C-MIND data used in the preparation of this article were obtained from the C-MIND Data Repository (accessed in February 2015) created by the C-MIND study of Normal Brain Development. This is a multisite, longitudinal study of typically developing children from ages newborn through young adulthood conducted by Cincinnati Children's Hospital Medical Center and UCLA A listing of the participating sites and a complete listing of the study investigators can be found at https://research.cchmc.org/c-mind.

The NDAR data used in the preparation of this manuscript were obtained from the NIH-supported National Database for Autism Research (NDAR). NDAR is a collaborative informatics system created by the National Institutes of Health to provide a national resource to support and accelerate research in autism. The NDAR dataset includes data from the NIH Pediatric MRI Data Repository created by the NIH MRI Study of Normal Brain Development. This is a multisite, longitudinal study of typically developing children from ages newborn through young adulthood conducted by the Brain Development Cooperative Group A listing of the participating sites and a complete listing of the study investigators can be found at http://pediatricmri.nih.gov/nihpd/info/participating_centers.html.

The ADNI data used in the preparation of this manuscript were obtained from the Alzheimer's Disease Neuroimaging Initiative (ADNI). The ADNI is funded by the National Institute on Aging and the National Institute of Biomedical Imaging and Bioengineering and through generous contributions from the following: Abbott, AstraZeneca AB, Bayer Schering Pharma AG, Bristol-Myers Squibb, Eisai Global Clinical Development, Elan Corporation, Genentech, GE Healthcare, GlaxoSmithKline, Innogenetics NV, Johnson & Johnson, Eli Lilly and Co., Medpace, Inc., Merck and Co., Inc., Novartis AG, Pfizer Inc., F. Hoffmann-La Roche, Schering-Plough, Synarc Inc., as well as nonprofit partners, the Alzheimer's Association and Alzheimer's Drug Discovery Foundation, with participation from the U.S. Food and Drug Administration. Private sector contributions to the ADNI are facilitated by the Foundation for the National Institutes of Health (www.fnih.org). The grantee organization is the Northern California Institute for Research and Education, and the study was coordinated by the Alzheimer's Disease Cooperative

Study at the University of California, San Diego. ADNI data are disseminated by the Laboratory for NeuroImaging at the University of California, Los Angeles.

The OASIS data used in the preparation of this manuscript were obtained from the OASIS project. See http://www.oasis-brains.org/for more details. The AIBL data used in the preparation of this manuscript were obtained from the AIBL study of ageing. See www.aibl.csiro.au for further details. The ICBM data used in the preparation of this manuscript. The IXI data used in the preparation of this manuscript were supported by the - http://www.brain-development.org/.

The ABIDE data used in the preparation of this manuscript were supported by ABIDE funding resources listed at http://fcon_1000.projects.nitrc.org/indi/abide/. ABIDE primary support for the work by Adriana Di Martino. Primary support for the work by Michael P. Milham and the INDI team was provided by gifts from Joseph P. Healy and the Stavros Niarchos Foundation to the Child Mind Institute. http://fcon_1000.projects.nitrc.org/indi/abide/ This manuscript reflects the views of the authors and may not reflect the opinions or views of the database providers.

REFERENCES

Ashburner J, Friston KJ (2005): Unified segmentation. Neuroimage 26:839–851.

Aubert-Broche B, Fonov VS, Garcia-Lorenzo D, Mouiha A, Guizard N, Coupe P, Eskildsen SF, Collins DL (2013): A new method for structural volume analysis of longitudinal brain MRI data and its application in studying the growth trajectories of anatomical brain structures in childhood. Neuroimage 82:393–402.

Avants BB, Tustison NJ, Song G, Cook PA, Klein A, Gee JC (2011): A reproducible evaluation of ANTs similarity metric performance in brain image registration. Neuroimage 54:2033–2044.

Becker JB, Hu M (2008): Sex differences in drug abuse. Front Neuroendocrinol 29:36–47.

Brain Development Cooperative Group (2012): Total and regional brain volumes in a population-based normative sample from 4 to 18 years: The NIH MRI Study of Normal Brain Development. Cereb Cortex 22:1–12.

Carne RP, Vogrin S, Litewka L, Cook MJ (2006): Cerebral cortex: An MRI-based study of volume and variance with age and sex. J Clin Neurosci 13:60–72.

Coffey CE, Lucke JF, Saxton JA, Ratcliff G, Unitas LJ, Billig B, Bryan RN (1998): Sex differences in brain aging: A quantitative magnetic resonance imaging study. Arch Neurol 55:169–179.

Coupe P, Manjon JV, Fonov V, Pruessner J, Robles M, Collins DL (2011): Patch-based segmentation using expert priors: Application to hippocampus and ventricle segmentation. Neuroimage 54:940–954.

Ducharme S, Albaugh MD, Nguyen TV, Hudziak JJ, Mateos-Perez JM, Labbe A, Evans AC, Karama S, Brain Development Cooperative Group (2016): Trajectories of cortical thickness maturation in normal brain development—The importance of quality control procedures. Neuroimage 125:267–279.

Eriksson PS, Perfilieva E, Björk-Eriksson T, Alborn A-M, Nordborg C, Peterson DA, Gage FH (1998): Neurogenesis in the adult human hippocampus. Nat Med 4:1313–1317.

Fjell AM, Westlye LT, Amlien I, Espeseth T, Reinvang I, Raz N, Agartz I, Salat DH, Greve DN, Fischl B, Dale AM, Walhovd KB (2009): High consistency of regional cortical thinning in aging across multiple samples. Cereb Cortex 19:2001–2012.

Fjell AM, Westlye LT, Grydeland H, Amlien I, Espeseth T, Reinvang I, Raz N, Holland D, Dale AM, Walhovd KB, Alzheimer Disease Neuroimaging Initiative (2013): Critical ages in the life course of the adult brain: Nonlinear subcortical aging. Neurobiol Aging 34:2239–2247.

Fjell AM, McEvoy L, Holland D, Dale AM, Walhovd KB, Alzheimer's Disease Neuroimaging Initiative (2014): What is normal in normal aging? Effects of aging, amyloid and Alzheimer's disease on the cerebral cortex and the hippocampus. Prog Neurobiol 117:20–40.

Forlano PM, Woolley CS (2010): Quantitative analysis of pre- and postsynaptic sex differences in the nucleus accumbens. J Comp Neurol 518:1330–1348.

Fox N, Warrington E, Freeborough P, Hartikainen P, Kennedy A, Stevens J, Rossor MN (1996): Presymptomatic hippocampal atrophy in Alzheimer's disease. Brain 119:2001–2007.

Giedd JN, Rapoport JL (2010): Structural MRI of pediatric brain development: What have we learned and where are we going? Neuron 67:728–734.

Giedd JN, Blumenthal J, Jeffries NO, Castellanos FX, Liu H, Zijdenbos A, Paus T, Evans AC, Rapoport JL (1999): Brain development during childhood and adolescence: A longitudinal MRI study. Nat Neurosci 2:861–863.

Gilmore JH, Lin W, Prastawa MW, Looney CB, Vetsa YSK, Knickmeyer RC, Evans DD, Smith JK, Hamer RM, Lieberman JA (2007): Regional gray matter growth, sexual dimorphism, and cerebral asymmetry in the neonatal brain. J Neurosci 27: 1255–1260.

Gilmore JH, Shi F, Woolson SL, Knickmeyer RC, Short SJ, Lin W, Zhu H, Hamer RM, Styner M, Shen D (2012): Longitudinal development of cortical and subcortical gray matter from birth to 2 years. Cereb Cortex 22:2478–2485.

Good CD, Johnsrude IS, Ashburner J, Henson RN, Fristen KJ Frackowiak RS (2002). A voxel-based morphometric study of ageing in 465 normal adult human brains. In Biomedical Imaging, 2002. 5th IEEE EMBS International Summer School on (p 16). IEEE.

Green PS, Simpkins JW (2000): Neuroprotective effects of estrogens: Potential mechanisms of action. Int J Dev Neurosci 18:347–358.

Groeschel S, Vollmer B, King M, Connelly A (2010): Developmental changes in cerebral grey and white matter volume from infancy to adulthood. Int J Dev Neurosci 28:481–489.

Gur RC, Mozley PD, Resnick SM, Gottlieb GL, Kohn M, Zimmerman R, Herman G, Atlas S, Grossman R, Berretta D (1991): Gender differences in age effect on brain atrophy measured by magnetic resonance imaging. Proc Natl Acad Sci USA 88:2845–2849.

Hedman AM, van Haren NE, Schnack HG, Kahn RS, Pol H, Hilleke E (2012): Human brain changes across the life span: A review of 56 longitudinal magnetic resonance imaging studies. Hum Brain Mapp 33:1987–2002.

Holland D, Chang L, Ernst TM, Curran M, Buchthal SD, Alicata D, Skranes J, Johansen H, Hernandez A, Yamakawa R (2014): Structural growth trajectories and rates of change in the first 3 months of infant brain development. JAMA Neurol 71:1266–1274.

Hu S, Pruessner JC, Coupe P, Collins DL (2013): Volumetric analysis of medial temporal lobe structures in brain development from childhood to adolescence. Neuroimage 74:276–287.

Huttenlocher PR, Dabholkar AS (1997): Regional differences in synaptogenesis in human cerebral cortex. J Comp Neurol 387: 167–178.

Jack CR, Petersen RC, Xu YC, Waring SC, O'Brien PC, Tangalos EG, Smith GE, Ivnik RJ, Kokmen E (1997): Medial temporal atrophy on MRI in normal aging and very mild Alzheimer's disease. Neurology 49:786–794.

Jernigan TL, Baaré W, Stiles FJ, Madsen KS (2011): Postnatal brain development: Structural imaging of dynamic neurodevelopmental processes. Prog Brain Res 189:77.

Lebel C, Gee M, Camicioli R, Wieler M, Martin W, Beaulieu C (2012): Diffusion tensor imaging of white matter tract evolution over the lifespan. Neuroimage 60:340–352.

Lenroot RK, Giedd JN (2010): Sex differences in the adolescent brain. Brain Cogn 72:46–55.

Lenroot RK, Gogtay N, Greenstein DK, Wells EM, Wallace GL, Clasen LS, Blumenthal JD, Lerch J, Zijdenbos AP, Evans AC, Thompson PM, Giedd JN (2007): Sexual dimorphism of brain developmental trajectories during childhood and adolescence. Neuroimage 36:1065–1073.

Makropoulos A, Gousias IS, Ledig C, Aljabar P, Serag A, Hajnal JV, Edwards AD, Counsell SJ, Rueckert D (2014): Automatic whole brain MRI segmentation of the developing neonatal brain. IEEE trans Med Imaging 33:1818–1831.

Makropoulos A, Aljabar P, Wright R, Huning B, Merchant N, Arichi T, Tusor N, Hajnal JV, Edwards AD, Counsell SJ, Rueckert D (2016): Regional growth and atlasing of the developing human brain. Neuroimage 125:456–478.

Manjon JV, Coupe P (2016): volBrain: An online MRI brain volumetry system. Front Neuroinform 10:30.

Manjon JV, Coupe P, Marti-Bonmati L, Collins DL, Robles M (2010a): Adaptive non-local means denoising of MR images with spatially varying noise levels. J Magn Reson Imaging 31: 192–203.

Manjón JV, Tohka J, Robles M (2010b): Improved estimates of partial volume coefficients from noisy brain MRI using spatial context. Neuroimage 53:480–490.

Manjon JV, Eskildsen SF, Coupe P, Romero JE, Collins DL, Robles M (2014): Nonlocal intracranial cavity extraction. Int J Biomed Imaging 2014:820205.

Mills KL, Goddings A-L, Herting MM, Meuwese R, Blakemore S-J, Crone EA, Dahl RE, Güroğlu B, Raznahan A, Sowell ER (2016): Structural brain development between childhood and adulthood: Convergence across four longitudinal samples. NeuroImage 141:273–281.

Ostby Y, Tamnes CK, Fjell AM, Westlye LT, Due-Tonnessen P, Walhovd KB (2009): Heterogeneity in subcortical brain development: A structural magnetic resonance imaging study of brain maturation from 8 to 30 years. J Neurosci 29: 11772–11782.

Paxinos G, Mai JK (2004): The Human Nervous System, Academic Press.

Pfefferbaum A, Rohlfing T, Rosenbloom MJ, Chu W, Colrain IM, Sullivan EV (2013): Variation in longitudinal trajectories of regional brain volumes of healthy men and women (ages 10 to 85 years) measured with atlas-based parcellation of MRI. Neuroimage 65:176–193.

Phelps EA, LeDoux JE (2005): Contributions of the amygdala to emotion processing: From animal models to human behavior. Neuron 48:175–187.

Poldrack RA, Gorgolewski KJ (2014): Making big data open: Data sharing in neuroimaging. Nat Neurosci 17:1510–1517.

Potvin O, Mouiha A, Dieumegarde L, Duchesne S and I. Alzheimer's Disease Neuroimaging (2016): Normative data for subcortical regional volumes over the lifetime of the adult human brain. Neuroimage 137:9–20.

Potvin O, Dieumegarde, Duchesne LS, Alzheimer's Disease Neuroimaging Initiative (2017): Freesurfer cortical normative data for adults using Desikan-Killiany-Tourville and ex vivo protocols. NeuroImage 156:43–64.

Raznahan A, Shaw P, Lalonde F, Stockman M, Wallace GL, Greenstein D, Clasen L, Gogtay N, Giedd JN (2011): How does your cortex grow? J Neurosci 31:7174–7177.

Shaw P, Kabani NJ, Lerch JP, Eckstrand K, Lenroot R, Gogtay N, Greenstein D, Clasen L, Evans A, Rapoport JL (2008): Neurodevelopmental trajectories of the human cerebral cortex. J Neurosci 28:3586–3594.

Sowell ER, Peterson BS, Thompson PM, Welcome SE, Henkenius AL, Toga AW (2003): Mapping cortical change across the human life span. Nat Neurosci 6:309–315.

Spalding KL, Bergmann O, Alkass K, Bernard S, Salehpour M, Huttner HB, Bostrom E, Westerlund I, Vial C, Buchholz BA, Possnert G, Mash DC, Druid H, Frisen J (2013): Dynamics of hippocampal neurogenesis in adult humans. Cell 153: 1219–1227.

Stiles J, Jernigan TL (2010): The basics of brain development. Neuropsychol Rev 20:327–348.

Suzuki M, Hagino H, Nohara S, Zhou S-Y, Kawasaki Y, Takahashi T, Matsui M, Seto H, Ono T, Kurachi M (2005): Male-specific volume expansion of the human hippocampus during adolescence. Cereb Cortex 15:187–193.

Tottenham N, Sheridan MA (2009): A review of adversity, the amygdala and the hippocampus: A consideration of developmental timing. Front Hum Neurosci 3:68.

Tustison NJ, Avants BB, Cook PA, Zheng Y, Egan A, Yushkevich PA, Gee JC (2010): N4ITK: Improved N3 bias correction. IEEE Trans Med Imaging 29:1310–1320.

van Praag H, Schinder AF, Christie BR, Toni N, Palmer TD, Gage FH (2002): Functional neurogenesis in the adult hippocampus. Nature 415:1030–1034.

Vijayakumar N, Allen NB, Youssef G, Dennison M, Yucel M, Simmons JG, Whittle S (2016): Brain development during adolescence: A mixed-longitudinal investigation of cortical thickness, surface area, and volume. Hum Brain Mapp 37: 2027–2038.

Walhovd KB, Westlye LT, Amlien I, Espeseth T, Reinvang I, Raz N, Agartz I, Salat DH, Greve DN, Fischl B, Dale AM, Fjell AM (2011): Consistent neuroanatomical age-related volume differences across multiple samples. Neurobiol Aging 32:916–932.

Walhovd KB, Fjell A, Giedd MJ, Dale AM, Brown TT (2016): Through thick and thin: A need to reconcile contradictory results on trajectories in human cortical development. Cereb Cortex 27:1472.

Wang L, Shi F, Li G, Gao Y, Lin W, Gilmore JH, Shen D (2014): Segmentation of neonatal brain MR images using patch-driven level sets. NeuroImage 84:141–158.

Yushkevich PA, Piven J, Hazlett HC, Smith RG, Ho S, Gee JC, Gerig G (2006): User-guided 3D active contour segmentation of anatomical structures: Significantly improved efficiency and reliability. Neuroimage 31:1116–1128.

Ziegler G, Dahnke R, Jancke L, Yotter RA, May A, Gaser C (2012): Brain structural trajectories over the adult lifespan. Hum Brain Mapp 33:2377–2389.